TABLE 2 Amino acid sequence homologies of the polyproteins

	Non-primate hepaciviruses					
	H10-094 (JQ434007)	B10-022 (JQ434004)	NZP1 (JQ434001)	AAK-2011 (JF44991)	H3-011 (JQ434008)	A6-066 (JQ434003)
JPN3/JAPAN/2013 (AB863589)	97.8[a]	96.7	95.7	95.7	95.6	95.3

	Non-primate hepaciviruses		HCV			
	G1-073 (JQ434002)	F8-068 (JQ434005)	HCV1a (NC004102)	HCV1b (AB779562)	JFH1 (AB047639)	GBV-B (NC001655)
JPN3/JAPAN/2013 (AB863589)	94.9	94.1	46.5	45.6	44.5	28.9

	Non-primate hepaciviruses		
	JPN3/JAPAN/2013 (AB863589)	AAK-2011 (JF44991)	GBV-B (NC001655)
HCV1a (NC004102)	46.1	46.0	33.3

[a], percent identity.

trees of the NS3 (Fig. 3A) and NS5B regions (Fig. 3B) showed that JPN3/JAPAN/2013 was included in the clade comprising the U.S. strains NPHV-H10-094 (GenBank accession number JQ434007) and B10-022 (GenBank accession number JQ434004).

Putative RNA secondary structures around the UTRs of EHcV. The 5′-terminal region of JPN3/JAPAN/2013 was compared with those of the EHcV genomes (Fig. 4A). The HCV internal ribosome entry site (IRES)-like structure was embedded in the 5′ UTRs of NPHVs (5, 6). The 5′-UTR region was well conserved among the EHcV strains and showed a mean diversity of approximately 4% among the EHcV strains (Fig. 4A). The 3′-terminal sequence downstream of the (A)-rich region in the EHcV genome had not been reported because the (A)-rich region downstream of the stop codon of EHcV interrupted the reaction in the ordinary 3′-RACE method (5, 6). In the present study, we determined the nucleotide sequences downstream of the (A)-rich region from serum sample 3 (JPN3/JAPAN/2013; GenBank accession number AB863589), sample 5 (JPN5/JAPAN/2015; GenBank accession number AB921150), and sample 1 (JPN1/JAPAN/2015; GenBank accession number AB921151) by the modified 3′-RACE method using poly(U) polymerase, although the region in serum sample 1 was incompletely amplified (Fig. 4B). The regions downstream of the (A)-rich region were conserved between serum samples 3 and 5, whereas the (A)-rich regions varied among the three strains (Fig. 4B).

The secondary structure of 5′ UTR in strain JPN3/JAPAN/2013 was predicted according to the method described previously (8) (Fig. 4C). The stem-loops in the 5′ UTR were designated according to the stem-loops of the HCV 5′-UTR structures (30). Stem-loops (SLs) I, II, IIIa to IIIf, and the pseudoknot interaction were predicted within the 5′ UTR of strain JPN3/JAPAN/2013. These structures were the same as that of the strain reported previously (9), although several nucleotide insertions and deletions were more predominant in the apical loop of subdomain IIIb than in the other strains reported previously (Fig. 4A and C). Two seed sites of the microRNA miR-122 (Fig. 4A and C) were found in the 5′ UTR of strain JPN3/JAPAN/2013 at nucleotide residues 81 to 89 (UCCACAUUA) and 98 to 103 (CACUCC), which also corresponded to the predicted miR-122 seed sites in the 5′ UTRs of the other EHcV strains (9).

The HCV 3′ UTR, which is generally 200 to 300 nucleotides in length, consists of a short variable region, the poly(U/UC) stretch sequence, and the 3′-X-tail region, in that order (31–33). Although the EHcV 3′ UTR, which is composed of 138 nucleotides, is shorter than the HCV 3′ UTR, the 3′ UTR of EHcV consists of the (A)-rich sequence and 3′-X-tail region, in that order. The (A)-rich sequence of EHcV may vary in length (Fig. 4B). We subsequently predicted the secondary structure of the EHcV 3′ UTR. Although the EHcV 3′ UTR, which is composed of 138 nucleotides, is shorter than the HCV 3′ UTR, the 3′ UTR includes three predicted SL structures (Fig. 4C). Based on the SL structures in the HCV 3′ X-tail, these SL structures in the EHcV 3′ UTR were designated 3′SL I, 3′SL II, and 3′SL III, in that order from the 3′ terminus (Fig. 4C). Interestingly, the (A)-rich sequence was partially incorporated into the 3′SL III, although the poly(U/UC) stretch sequence in the HCV 3′ UTR is separated from any 3′SL structures (31–33). Furthermore, the two SL structures in the 3′ side of the EHcV NS5B-coding region were predicted to correspond to 5BSL3.2 and 5BSL3.3 in the NS5B-coding region of HCV. HCV 5BSL3.2 was previously shown to interact with 3′SL II to form the kissing-loop interaction, which is required for HCV replication (33). The secondary structure prediction shown in Fig. 4C suggests that the kissing-loop interaction may be conserved between 5BSL3.2 and the 3′SL II of the EHcV genome through their complementary sequences. The long-range RNA-RNA interaction between the apical loop of subdomain IIId in HCV IRES and the bulge of 5BSL3.2 supports IRES-dependent translation and viral RNA replication (34–36). In the case of the EHcV genome, the complement sequences were detected in the apical loops of subdomain and the 5BSL3.2-like subdomain (Fig. 4C), suggesting that the long-range RNA-RNA interaction may reside in the EHcV genome. These results indicated that HCV-like RNA secondary structures may be conserved around both UTRs of the EHcV genome.

Cleavage of the EHcV core protein by SPP. The C-terminal transmembrane region of the HCV core protein was previously shown to be cleaved by SPP following the cleavage of the core-E1 junction by signal peptidase (11, 28, 37). The core protein is known to be released from the precursor polyprotein embedded in the endoplasmic reticulum (ER) membrane, and it then moves

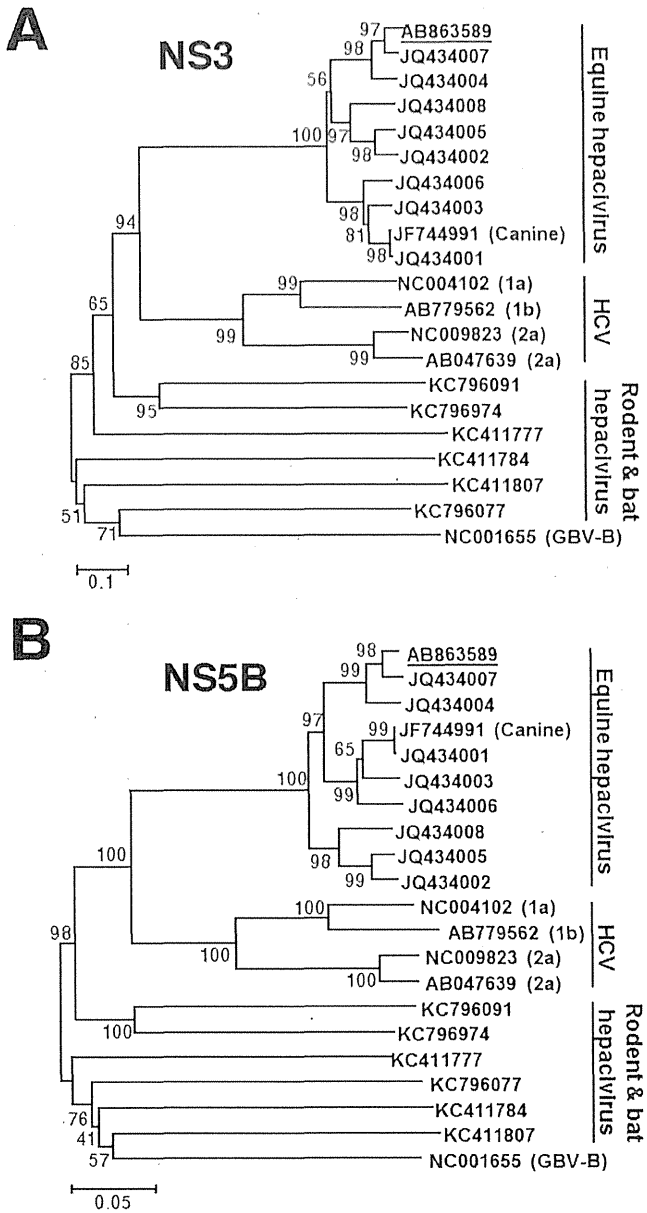

FIG 3 Phylogenetic analysis of the EHcV gene. Neighbor-joining trees of the nucleotide sequences from the NS3 (A) and NS5B (B) regions of the NPHV, HCV, and GBV-B strains are shown (23). Trees were constructed by the maximum composite likelihood method calculated using the program MEGA5 (24). The percentage of replicate trees in which the associated taxa were clustered together in the bootstrap test (1,000 replicates) is indicated next to the branches. Analyses were carried out using 10 strains of EhcV, JPN3/JAPAN/2013, A6-066 (GenBank accession no. JQ434003), B10-022 (GenBank accession no. JQ434004), F8-068 (GenBank accession no. JQ434005), G1-073 (GenBank accession no. JQ434002), G5-077 (GenBank accession no. JQ434006), H3-011 (GenBank accession no. JQ434008), H10-094 (GenBank accession no. JQ434007), NZP1 (GenBank accession no. JQ434001), and AAK-2011 (canine hepacivirus; GenBank accession no. JF744991); 4 strains of HCV, H77 (genotype 1a; GenBank accession no. NC004102), LyHCV (genotype 1b; GenBank accession no. AB779562), HC-J6CH (genotype 2a; GenBank accession no. NC009823), and JFH1 (genotype 2a; GenBank accession no. AB047639); 3 strains of bat hepacivirus, PDB-112 (GenBank accession no. KC796077), PDB-445 (GenBank accession no. KC796091), and PDB-829 (GenBank accession no. KC796074); 3 strains of rodent hepacivirus, RMU10-3382 (GenBank accession no. KC411777), NLR-AP-70 (GenBank accession no. KC411784), and SAR-46 (GenBank accession no. KC411807); and another primate hepacivirus, GBV-B (GenBank accession no. NC001655). The Japanese strain JPN3/JAPAN/2013 (GenBank accession no. AB863589) is underlined.

mainly to lipid droplets (LDs) (13, 14). Although SPP-dependent cleavage and LD translocation of the capsid protein are features common to HCV and GBV-B (13), it currently remains unknown whether the EHcV core protein shows these properties. The EHcV core protein shared 49.5% amino acid homology with the HCV core protein (genotype 1b) (Fig. 5A) and exhibited a hydrophobic/hydrophilic pattern similar to that of the HCV core protein (Fig. 5B). The EHcV core protein was predicted to be composed of domains 1, 2, and 3 relative to the HCV core protein. The transmembrane region of the EHcV core protein was predicted to span from Asn^{177} to Val^{199} by TMHMM2.0 (http://www.cbs.dtu.dk/services/TMHMM/). The transmembrane region of the EHcV core protein was 65% identical to that of the HCV core proteins (Fig. 5A). The C-terminal residue of the mature HCV core protein was found to be Phe^{177} in human and insect cell lines (17, 38). Our previous findings suggest that Ile^{176} and Phe^{177} of the HCV core protein may be responsible for SPP-dependent cleavage, because the replacement of Ile^{176} and Phe^{177} with Ala and Leu, respectively, abrogated intramembrane cleavage by SPP and impaired virus production (17, 28, 39). Weihofen et al. reported that SPP cleaved a peptide bond of the alpha-helix-breaking structure in a transmembrane region of the membrane protein (40). The replacement of Ile^{176} and Phe^{177} with Ala and Leu, respectively, in the HCV core protein converted the beta-sheet structure (alpha-helix-breaking structure) to an alpha-helix structure in the transmembrane region, as reported previously (28) (Fig. 6A and B). Ile^{190} and Phe^{191} of the EHcV core protein, which correspond to Ile^{176} and Phe^{177}, respectively, of the HCV core protein, reside in the alpha-helix-breaking structure of the transmembrane region (Fig. 6A and B). In contrast, the replacement of Ile^{190} and Phe^{191} with Ala and Leu, respectively, in the EHcV core protein were predicted to convert the beta-sheet to an alpha-helix structure in a manner similar to that for the HCV core protein (Fig. 6A and B). To investigate the involvement of SPP in the maturation of the EHcV core protein, we expressed EHcVc or HCVc in 293FT cells with an SPP or SPP mutant. These core proteins were expected to be resistant to signal peptidase-dependent processing because the C-terminal residue Ala of both core proteins was replaced with Arg, resulting in the detection of an immature core protein by the anti-HA antibody (Fig. 6A) (28). The core proteins with molecular masses of 23 kDa and 28 kDa were detected mainly with the anti-FLAG antibody in 293FT cells expressing HCVc and HCVc-mt, respectively (Fig. 6C, lanes 2 and 3); however, the 23-kDa band was not detected with the anti-HA antibody (Fig. 6C, lane 2). When EHcVc was expressed in 293FT cells, it was detected at a molecular mass of 27 kDa with the anti-FLAG antibody, but not with the anti-HA antibody (Fig. 6C, lane 4). In contrast, EHcV-mt, in which the 190th and 191st residues were Ala and Leu instead of Ile and Phe, respectively, was detected mainly at a molecular mass of 30 kDa with the anti-FLAG and anti-HA antibodies (Fig. 6C, lane 5). A loss-of-function SPP mutant (SPP-D219A) in which the 219th residue was Ala instead of Asp was shown to have a dominantly negative effect on SPP-dependent cleavage of the

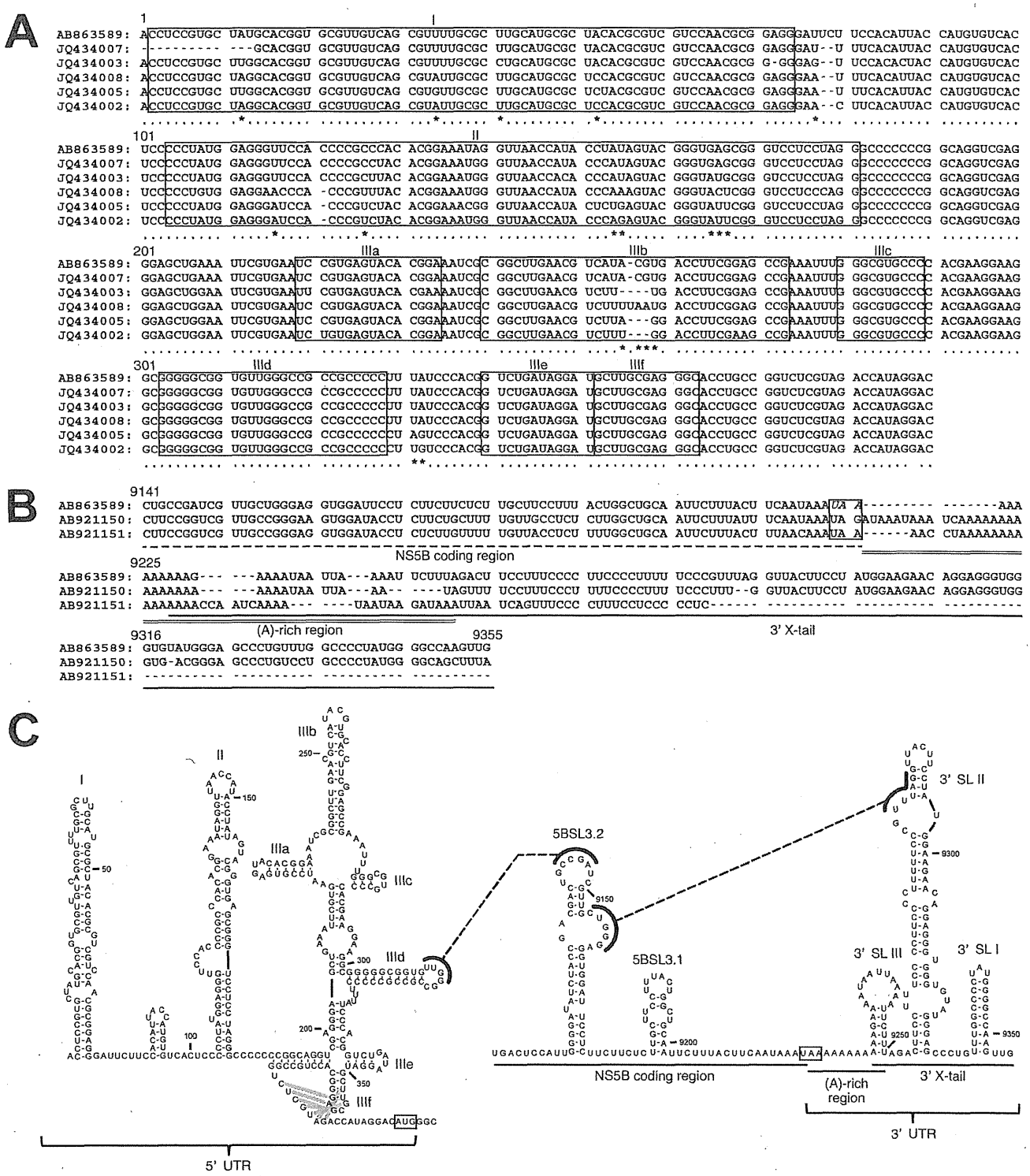

FIG 4 RNA structure analysis of the 5′ and 3′ ends of EHcV. (A) Alignment of the 5′ UTRs of the EHcV strains. Asterisks and black lines indicate variable residues and miRNA-targeting regions, respectively. SL structures are enclosed in rectangles. GenBank numbers are listed in the legend to Fig. 3. (B) Alignment of the 3′ UTRs of the EHcV strains. The 3′-terminal sequences with GenBank numbers AB921150 and AB921151 were determined using serum samples 5 and 1, respectively, and were aligned with that of JPN3/JAPAN/2013 (GenBank accession no. AB863589). (C) The secondary structures of the 5′ UTR, NS5B-coding region, and 3′ UTR were predicted on the basis of minimum free energy predictions. The stem loops in the 5′ UTR (left) were designated according to the stem loops of the HCV 5′-UTR structures (30). A gray line, double line, and single line indicate a pseudoknot structure, miR-122-target region, and complementary sequence, respectively. The stem loops in the NS5B-coding region and 3′ UTR (right) were designated to correspond to the stem loops embedded in the HCV 3′-terminal region (32, 33). The NS5B-coding region, (A)-rich region, and 3′-X-tail sequence are indicated under the schematic structure. Start and stop codons are enclosed by rectangles.

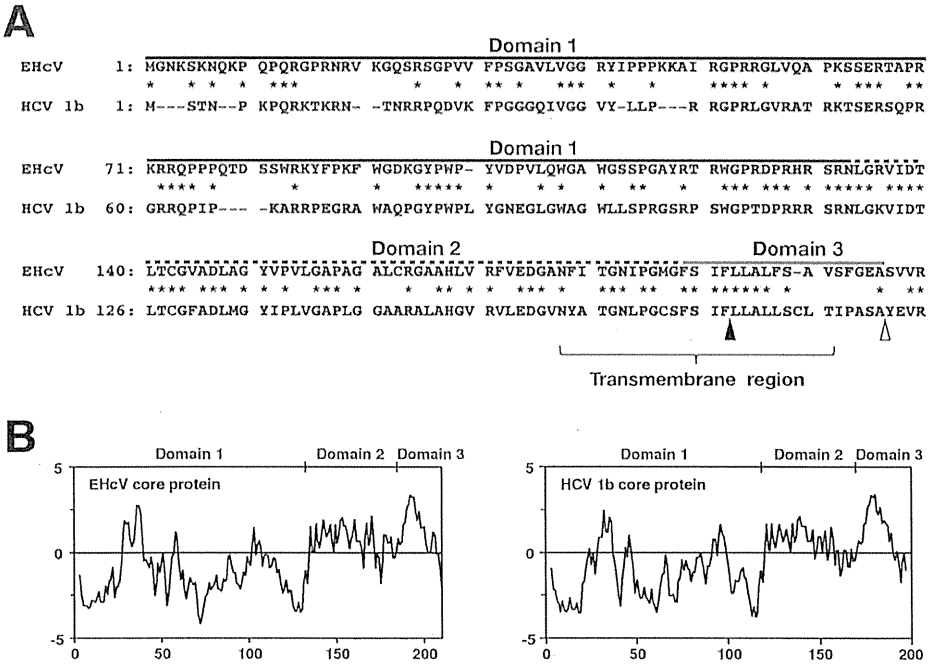

FIG 5 Amino acid alignment and hydrophobicity of EHcV and HCV core proteins. (A) Alignment of the core proteins of EHcV (JPN3/JAPAN/2013) and HCV genotype1b (Con1; GenBank accession number AJ238799). Asterisks indicate identical amino acid residues. Bars indicate gaps to achieve maximum amino acid matching. The black and white arrowheads indicate the predicted cleavage site of the core protein of HCV by SPP and signal peptidase, respectively. The EHcV core protein was composed of three domains, domain 1 (a black line, residues 2 to 132), domain 2 (a broken black line, residues 133 to 187), and domain 3 (a gray line, residues 188 to 204), relative to those of the HCV core protein (42). (B) Hydrophobicity plots of the EHcV and HCV core proteins were prepared by the method of Kyte and Doolittle (26). The horizontal and vertical axes represent amino acid position and hydrophobicity, respectively.

HCV core protein and to be coprecipitated with the immature core protein (28). HCVc had a molecular mass of 23 kDa in the presence of wild-type SPP (SPP-wt) and was detected with the anti-FLAG antibody, but not with the anti-HA antibody (Fig. 6D, lane 2), suggesting that the 23-kDa protein band may be a mature core protein. HCVc mainly had a molecular mass of 28 kDa in the presence of SPP-D219A and was detected with the anti-FLAG and anti-HA antibodies (Fig. 6D, lane 3), which corresponds to the mobility of HCVc-mt (Fig. 6D, lane 4). These results suggest that SPP-D219A may abrogate the intramembrane cleavage of HCVc. In a manner similar to that for the HCV core protein, EHcVc was detected mainly at a molecular mass of 27 kDa in the presence of SPP-wt with the anti-FLAG antibody, but not with the anti-HA antibody (Fig. 6D, lane 6). EHcVc was detected mainly at a molecular mass of 30 kDa in the presence of SPP-D219A with anti-FLAG and anti-HA antibodies (Fig. 6D, lane 7), corresponding to the mobility of EHcVc-mt (Fig. 6D, lane 8). When SPP-D219A was coexpressed with either HCVc or EHcVc, immature HCVc and EHcVc were coprecipitated with SPP-D219A (Fig. 6E, lanes 3 and 5). These results suggest that the EHcV core protein may be cleaved by SPP and that Ile^{190} and Phe^{191} of the EHcV core protein are critical for SPP-dependent cleavage.

The intracellular localization of the hepacivirus core protein. The HCV core protein is known to be localized mainly on the surface of LDs and is partially fractionated in the detergent-resistant membrane (DRM) close to the budding sites on the ER (13, 14, 16, 17). The core protein is considered to encompass the viral genome on the ER membrane, followed by budding into the lumen side (13, 14, 16, 17). To examine the intracellular localization of the EHcV core protein, we expressed HCVc or EHcVc in the Huh7OK1 cell line and stained the core proteins with the anti-FLAG antibody after staining LDs. Consistent with the findings of previous studies (14, 41, 42), HCVc was localized mainly on LDs (Fig. 7, row 3), whereas HCV-mt was not (Fig. 7, row 4). In a manner similar to that for the HCV core protein, EHcVc was localized mainly on LDs (Fig. 7, top row), whereas EHcVc-mt was not (Fig. 7, second row). These results suggest that the EHcV core protein may be localized mainly on LDs after SPP-dependent cleavage.

The DRM is defined as the cholesterol/sphingolipid-rich microdomain, which is resistant to nonionic detergents such as Triton X-100, considered to be a characteristic of lipid rafts. HCV was previously shown to be propagated in lipid raft-like compartments, including the membranous web (43–45). Furthermore, the HCV core protein is known to be associated with lipid raft-like compartments as well as LDs (16, 17, 41, 42). Therefore, we determined whether the EHcV core protein could be detected in the DRM fractions. EHcVc or EHcVc-mt was expressed in 293FT cells. The resulting cells were lysed on ice in the presence or absence of 1% Triton X-100. The DRM fractions were separated from the soluble proteins by a flotation assay with a stepwise density gradient in the presence or absence of Triton X-100. Serial fractions were collected after ultracentrifugation and were then subjected to Western blot analysis after being concentrated. EHcVc and EHcVc-mt were fractionated broadly from fractions of samples 3 to 11 without Triton X-100, and the fraction from

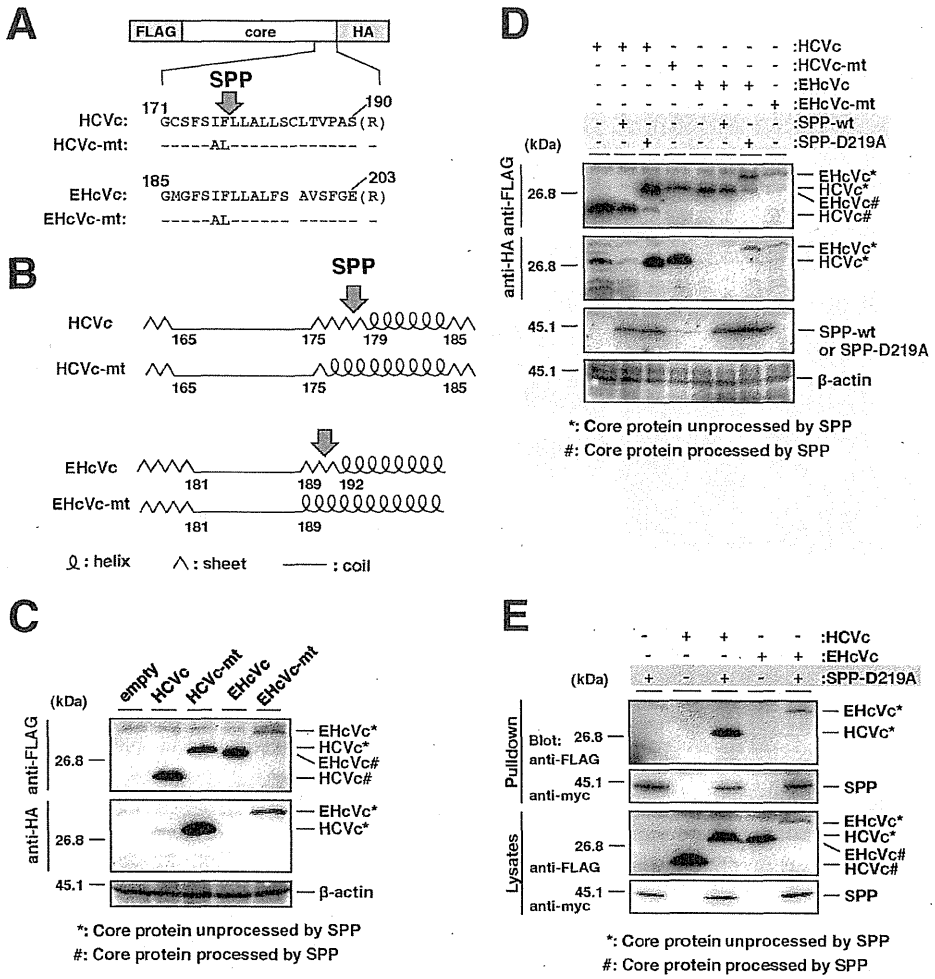

FIG 6 Intramembrane processing of the EHcV core protein by SPP. (A) The plasmids encoding HCVc, HCVc-mt, EHcVc, and EHcVc-mt are shown as a schematic diagram. Their C-terminal regions (171 to 190, HCV core protein; 185 to 203, EHcV core protein) were aligned. The C-terminal Ala of each core protein was replaced with Arg (R) to prevent signal peptidase-dependent cleavage for the detection of the SPP-uncleaved core protein with the anti-HA antibody. Bars indicate the amino acids that were the same as those of the wild-type residues. (B) The secondary protein structures in the C-terminal transmembrane regions of the HCV and EHcV core proteins and mutants were predicted by the method of Garnier et al. (25). Arrows indicate putative SPP cleavage sites. (C) HCVc, HCVc-mt, EHcVc, and EHcVc-mt were expressed in 293FT cells and immunoblotted with the anti-FLAG and -HA antibodies. (D) HCVc or EHcVc was expressed with SPP-wt or SPP-D219A in the 293FT cell line. HCVc-mt and EHcVc-mt were expressed in the absence of SPP-wt and SPP-D219A as uncleavable controls. (E) HCVc or EHcVc was coexpressed with or without SPP-D219A. SPP-D219A was pulled down with Ni beads. Coprecipitated proteins were immunoblotted with the anti-FLAG antibody.

sample 8 contained the largest amount of the core protein (Fig. 8, left panels). The distributions of the core proteins were roughly consistent with that of calreticulin, a marker protein of the ER membrane. When the cells expressing EHcVc were lysed in the presence of Triton X-100, a large amount of the core protein was localized in fractions 9 to 11 (Fig. 8, top three panels on the right). These fractions were enriched in calreticulin, corresponding to the detergent-soluble fractions (Fig. 8, fractions 7 to 11, top three panels on the right). However, EHcVc was partially detected in fractions 3 to 6 together with caveolin-1, a marker protein of the lipid raft (Fig. 8, fractions 3 to 6, top three panels on the right), suggesting that the EHcV core protein may have been partially distributed in the DRM fractions. In contrast, EHcVc-mt was localized in the detergent-soluble fractions (Fig. 8, fractions 9 to 11, bottom three panels on the right), but not in the DRM fractions (Fig. 8, fractions 3 to 6, bottom three panels on the right), in the presence of Triton X-100. EHcVc-mt was resistant to SPP-dependent processing, as described above (Fig. 6). These results suggest that the EHcV core protein may have been partially localized in the DRM and also that SPP-dependent processing may be required for DRM localization of the EHcV core protein.

DISCUSSION

The results of the present study indicate that EHcV infects Japanese-born domestic horses. Previous studies suggested that EHcV infected mainly horses and rarely dogs (5, 7–9). Our results demonstrate that EHcV commonly infects Japanese-born domestic horses (35.6% PCR positive and 22.6% seropositive). Several groups reported a prevalence of less than 10% PCR positivity in horses raised in the United States, the United Kingdom, and Ger-

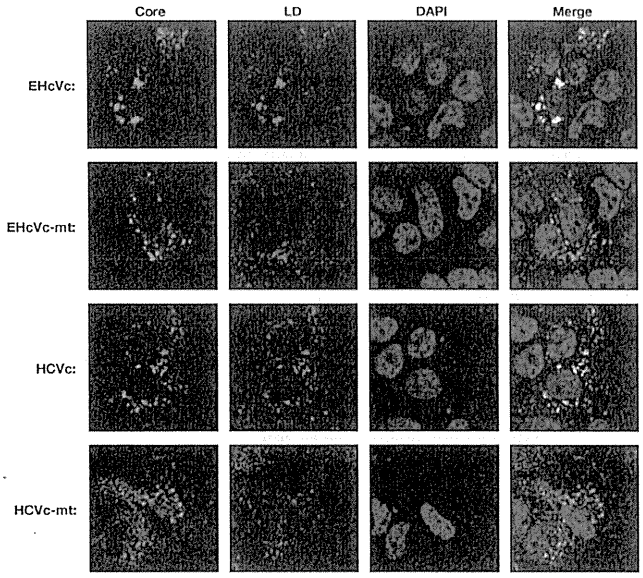

FIG 7 Intracellular localization of hepacivirus core proteins. HCVc, HCVc-mt, EHcVc, or EHcVc-mt was expressed in the Huh7OK1 cell line. The resulting cells were stained with Bodipy 558/568 (red) and then fixed with 4% paraformaldehyde at 24 h posttransfection, permeabilized, and subjected to indirect immunofluorescence staining. Each core protein was detected using mouse anti-FLAG antibodies and then Alexa 488-conjugated anti-mouse IgG (green). Cell nuclei were stained with DAPI after fixation (blue).

many (5, 7–9). Although the infection route of EHcV remains unknown, horses that were previously imported to Japan may be highly infected with EHcV. The serological prevalence in the present study appeared to be lower than that reported previously (8). A specific signal of the viral protein may be selected by Western blotting, used herein, rather than by the luciferase immunoprecipitation system, as reported previously (8), since the serum of each horse reacted to different proteins irrespective of the EHcV core protein (Fig. 2). The predicted full sequence of the EHcV strain amplified from serum sample 3 had high homology to those of the previously reported strains (Table 2). The polyproteins of previous strains had approximately 95% amino acid homology to one another irrespective of the area in which the horses originated, suggesting that these strains may belong to the same virological species. The parents of horse number 3 were born in Japan, while its grandparents were imported from the United States and Canada. Unfortunately, the sera of the parents and grandparents were not obtained in the present study. The EHcV strains obtained from Japanese-born horses may have originated from the United States or Canada. Another possibility is that one species of EHcV may have recently been distributed worldwide.

The primary and secondary structures of both UTRs are conserved among HCV strains and are essential for replication and translation. Four major stem-loop (SL) motifs have been detected in the 5′ UTR of the HCV genome, three SL structures of which are known to be required for IRES activity (46). Domain IIId plays a crucial role in anchoring of the 40S ribosome for IRES activity (47). Domain IIIb and the four-way helical junction of domains IIIa, IIIb, and IIIc bind eukaryotic initiation factor 3 (eIF3) and form a ternary complex, thereby forming the 48S preinitiation complex on HCV RNA (48). Moreover, domain II is known to be required to enhance eIF5-mediated GTP hydrolysis and the release of eIF2 from the 48S complex (48). These equivalent motifs were observed in the predicted secondary structures of the 5′ UTR of the reported EHcV strains (49), as well as in strain JPN3/JAPAN/2013 in the present study (Fig. 4C). A recent study demonstrated that the EHcV 5′ UTR exhibited IRES-dependent translation activity (50); however, further studies are needed to fully understand the IRES activity of the EHcV 5′UTR.

SL motifs embedded in the NS5B-coding region and UTRs of the HCV genome are known to be associated with viral replication. Several studies found that the mutational disruption of the complement sequence between 5BSL3.2 and 3′SL2 inhibited HCV RNA replication (33, 51). Additionally, the apical loop of domain IIId in the HCV 5′ UTR was shown to interact with the bulge of 5BSL3.2, supporting IRES-dependent translation and viral RNA replication (34–36). The RNA secondary structures of the 3′ UTR in the EHcV genome remained unknown due to limited information on its nucleotide sequence. 3′ RACE using poly(U) polymerase was employed in the present study because the ordinary 3′-RACE reaction using poly(A) polymerase was stopped at the (A)-rich region of the EHcV 3′ UTR. The nucleotide sequence of the EHcV 3′ UTR was determined, and its RNA secondary structure was then predicted (Fig. 4B and C). The results of the present

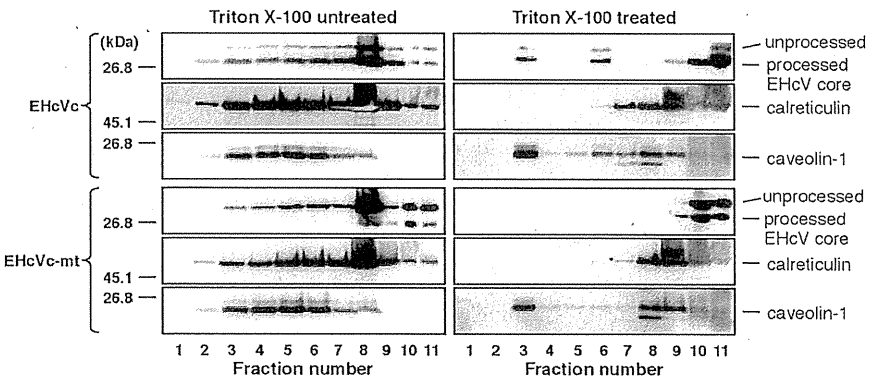

FIG 8 The EHcV core protein partially migrated to the DRM fraction after SPP-dependent processing. 293FT cells expressing either EHcVc or EHcVc-mt were homogenized with or without 1% Triton X-100 and then subjected to a flotation assay. Proteins in each fraction were concentrated with cold acetone and then subjected to Western blotting using the anti-FLAG, anti-calreticulin, or anti-caveolin-1 antibody.

study revealed that the 3′ UTR of the EHcV genome consists of the (A)-rich sequence and relatively shorter 3′-X-tail sequence. The three SL structures of the EHcV 3′ UTR were similar to those of the HCV 3′ UTR but were markedly different from the 3′ UTRs of GBV-B and rodent hepaciviruses. Drexler et al. described the structural characteristics of the 5′ and 3′ UTRs in rodent hepacivirus as well as phylogenetic information, liver tropism, and the pathogenicity of the virus (5). The SL motifs embedded in the 3′ X-tails of rodent hepacivirus and GBV-B varied. The structures of the 3′ UTRs appeared to correspond to the phylogenetic relationship of the hepaciviruses (5). Figure 4C shows that there were two stem-loop structures within the NS5B-coding region of EHcV corresponding to 5BSL3.2 and 5BSL3.3 of HCV RNA. Complementary regions were observed between the 5BSL3.2-like domain and 3′SL2, as well as between the 5BSL3.2-like domain and domain IIId of the EHcV genome (Fig. 4B and C). The kissing-loop and long-range RNA-RNA interactions may be structurally conserved between EHcV and HCV. Functional analyses of the *cis*-acting elements of the EHcV genome will contribute to the establishment of an EHcV infection system.

The mature HCV core protein was previously shown to be generated from the viral precursor polyprotein by signal peptidase followed by SPP-dependent processing of the transmembrane region (52). The core proteins of HCV and GBV-B are known to be cleaved by SPP (12, 37). The transmembrane regions of both the HCV and EHcV core proteins were found to be structurally conserved, based on their amino acid sequences and hydrophobicity plots (Fig. 5A and B and Fig. 6B). The replacement of Ile^{190} and Phe^{191} with Ala and Leu, respectively, in the EHcV core protein abrogated the intramembrane processing of the EHcV core protein (Fig. 6C). The loss-of-function mutant of SPP inhibited intramembrane processing of the EHcV core protein (Fig. 6D). Furthermore, the loss-of-function mutant of SPP specifically interacted with an uncleaved form of the EHcV core protein (Fig. 6E). These results indicate that the transmembrane region of the EHcV core protein may have been cleaved by SPP. The mature HCV core protein is known to be translocated into LDs and partially on lipid raft-like membranes. Previous studies reported that the HCV core protein on the LDs may be recruited near the replication complex in the membranous web, which consists of cholesterol- and sphingolipid-rich lipid components (43–45). Viral assembly was shown to occur on the ER membrane close to LDs and the membranous web (14). In addition to the HCV core protein, the nonstructural proteins and viral RNA of HCV were detected in the DRM fractions. The HCV RNA polymerase NS5B was previously reported to interact with sphingomyelin (53). Furthermore, a serine palmitoyltransferase inhibitor suppressed HCV replication by disrupting the replication complex (53, 54). These findings indicate that the DRM is provided as a scaffold for the formation of the HCV replication complex (45, 54). In the present study, we showed that the mature EHcV core protein was localized mainly on LDs and partially on the DRM (Fig. 7 and 8). A mutational analysis of the EHcV core protein indicated that SPP-dependent cleavage may be required for the localization of the EHcV core protein on LDs and the DRM in a manner similar to that for the HCV core protein. In addition, the assembly mechanism of EHcV may be similar to that of HCV.

In conclusion, the results of the present study show that EHcV shares common features with the HCV genomic structure and the biological properties of the capsid protein. *In vivo* and *ex vivo* infection systems for EHcV have not yet been successfully established. SCID mice carrying chimeric human livers are currently employed as a small animal model for *in vivo* infection with HCV (55) but are not suitable for studies on immunity and pathogenicity due to an immunodeficiency. Chimpanzees are not yet available for *in vivo* HCV research. Further studies on the mechanisms underlying EHcV infection will contribute to the development of an *in vivo* surrogate model system for studying HCV immunity and pathogenicity.

ACKNOWLEDGMENTS

We thank M. Furugori for her secretarial work, I. Katoh for helpful discussions, and C. Endoh for technical assistance.

This work was supported by Grants-in-Aid from the Ministry of Health, Labor, and Welfare, Japan (H24-Kanen-008 and H25-Kanen-002 and -008); the Ministry of Education, Culture, Sports, Science, and Technology, Japan; and the Japan Science and Technology Agency (JST) (Houga-24659204).

REFERENCES

1. **Simons JN, Leary TP, Dawson GJ, Pilot-Matias TJ, Muerhoff AS, Schlauder GG, Desai SM, Mushahwar IK.** 1995. Isolation of novel virus-like sequences associated with human hepatitis. Nat. Med. 1:564–569. http://dx.doi.org/10.1038/nm0695-564.
2. **Beames B, Chavez D, Lanford RE.** 2001. GB virus B as a model for hepatitis C virus. ILAR J. 42:152–160. http://dx.doi.org/10.1093/ilar.42.2.152.
3. **Bukh J, Apgar CL, Govindarajan S, Purcell RH.** 2001. Host range studies of GB virus-B hepatitis agent, the closest relative of hepatitis C virus, in New World monkeys and chimpanzees. J. Med. Virol. 65:694–697. http://dx.doi.org/10.1002/jmv.2092.
4. **Quan PL, Firth C, Conte JM, Williams SH, Zambrana-Torrelio CM, Anthony SJ, Ellison JA, Gilbert AT, Kuzmin IV, Niezgoda M, Osinubi MO, Recuenco S, Markotter W, Breiman RF, Kalemba L, Malekani J, Lindblade KA, Rostal MK, Ojeda-Flores R, Suzan G, Davis LB, Blau DM, Ogunkoya AB, Alvarez Castillo DA, Moran D, Ngam S, Akaibe D, Agwanda B, Briese T, Epstein JH, Daszak P, Rupprecht CE, Holmes EC, Lipkin WI.** 2013. Bats are a major natural reservoir for hepaciviruses and pegiviruses. Proc. Natl. Acad. Sci. U. S. A. 110:8194–8199. http://dx.doi.org/10.1073/pnas.1303037110.
5. **Drexler JF, Corman VM, Muller MA, Lukashev AN, Gmyl A, Coutard B, Adam A, Ritz D, Leijten LM, van Riel D, Kallies R, Klose SM, Gloza-Rausch F, Binger T, Annan A, Adu-Sarkodie Y, Oppong S, Bourgarel M, Rupp D, Hoffmann B, Schlegel M, Kummerer BM, Kruger DH, Schmidt-Chanasit J, Setien AA, Cottontail VM, Hemachudha T, Wacharapluesadee S, Osterrieder K, Bartenschlager R, Matthee S, Beer M, Kuiken T, Reusken C, Leroy EM, Ulrich RG, Drosten C.** 2013. Evidence for novel hepaciviruses in rodents. PLoS Pathog. 9:e1003438. http://dx.doi.org/10.1371/journal.ppat.1003438.
6. **Kapoor A, Simmonds P, Scheel TK, Hjelle B, Cullen JM, Burbelo PD, Chauhan LV, Duraisamy R, Sanchez Leon M, Jain K, Vandegrift KJ, Calisher CH, Rice CM, Lipkin WI.** 2013. Identification of rodent homologs of hepatitis C virus and pegiviruses. mBio 4(2):e00216–13. http://dx.doi.org/10.1128/mBio.00216-13.
7. **Lyons S, Kapoor A, Sharp C, Schneider BS, Wolfe ND, Culshaw G, Corcoran B, McGorum BC, Simmonds P.** 2012. Nonprimate hepaciviruses in domestic horses, United Kingdom. Emerg. Infect. Dis. 18:1976–1982. http://dx.doi.org/10.3201/eid1812.120498.
8. **Burbelo PD, Dubovi EJ, Simmonds P, Medina JL, Henriquez JA, Mishra N, Wagner J, Tokarz R, Cullen JM, Iadarola MJ, Rice CM, Lipkin WI, Kapoor A.** 2012. Serology-enabled discovery of genetically diverse hepaciviruses in a new host. J. Virol. 86:6171–6178. http://dx.doi.org/10.1128/JVI.00250-12.
9. **Kapoor A, Simmonds P, Gerold G, Qaisar N, Jain K, Henriquez JA, Firth C, Hirschberg DL, Rice CM, Shields S, Lipkin WI.** 2011. Characterization of a canine homolog of hepatitis C virus. Proc. Natl. Acad. Sci. U. S. A. 108:11608–11613. http://dx.doi.org/10.1073/pnas.1101794108.
10. **van der Laan LJ, de Ruiter PE, van Gils IM, Fieten H, Spee B, Pan Q, Rothuizen J, Penning LC.** 5 June 2014. Canine hepacivirus and idiopathic

hepatitis in dogs from a Dutch cohort. J. Viral Hepat. http://dx.doi.org/10.1111/jvh.12268.
11. Hüssy P, Langen H, Mous J, Jacobsen H. 1996. Hepatitis C virus core protein: carboxy-terminal boundaries of two processed species suggest cleavage by a signal peptide peptidase. Virology 224:93–104. http://dx.doi.org/10.1006/viro.1996.0510.
12. Targett-Adams P, Schaller T, Hope G, Lanford RE, Lemon SM, Martin A, McLauchlan J. 2006. Signal peptide peptidase cleavage of GB virus B core protein is required for productive infection in vivo. J. Biol. Chem. 281:29221–29227. http://dx.doi.org/10.1074/jbc.M605373200.
13. Hope RG, Murphy DJ, McLauchlan J. 2002. The domains required to direct core proteins of hepatitis C virus and GB virus-B to lipid droplets share common features with plant oleosin proteins. J. Biol. Chem. 277:4261–4270. http://dx.doi.org/10.1074/jbc.M108798200.
14. Miyanari Y, Atsuzawa K, Usuda N, Watashi K, Hishiki T, Zayas M, Bartenschlager R, Wakita T, Hijikata M, Shimotohno K. 2007. The lipid droplet is an important organelle for hepatitis C virus production. Nat. Cell Biol. 9:1089–1097. http://dx.doi.org/10.1038/ncb1631.
15. Samsa MM, Mondotte JA, Iglesias NG, Assuncao-Miranda I, Barbosa-Lima G, Da Poian AT, Bozza PT, Gamarnik AV. 2009. Dengue virus capsid protein usurps lipid droplets for viral particle formation. PLoS Pathog. 5:e1000632. http://dx.doi.org/10.1371/journal.ppat.1000632.
16. Matto M, Rice CM, Aroeti B, Glenn JS. 2004. Hepatitis C virus core protein associates with detergent-resistant membranes distinct from classical plasma membrane rafts. J. Virol. 78:12047–12053. http://dx.doi.org/10.1128/JVI.78.21.12047-12053.2004.
17. Okamoto K, Mori Y, Komoda Y, Okamoto T, Okochi M, Takeda M, Suzuki T, Moriishi K, Matsuura Y. 2008. Intramembrane processing by signal peptide peptidase regulates the membrane localization of hepatitis C virus core protein and viral propagation. J. Virol. 82:8349–8361. http://dx.doi.org/10.1128/JVI.00306-08.
18. Aizaki H, Lee KJ, Sung VM, Ishiko H, Lai MM. 2004. Characterization of the hepatitis C virus RNA replication complex associated with lipid rafts. Virology 324:450–461. http://dx.doi.org/10.1016/j.virol.2004.03.034.
19. Egger D, Wolk B, Gosert R, Bianchi L, Blum HE, Moradpour D, Bienz K. 2002. Expression of hepatitis C virus proteins induces distinct membrane alterations including a candidate viral replication complex. J. Virol. 76:5974–5984. http://dx.doi.org/10.1128/JVI.76.12.5974-5984.2002.
20. Marchuk D, Drumm M, Saulino A, Collins FS. 1991. Construction of T-vectors, a rapid and general system for direct cloning of unmodified PCR products. Nucleic Acids Res. 19:1154. http://dx.doi.org/10.1093/nar/19.5.1154.
21. Tajima S, Takasaki T, Matsuno S, Nakayama M, Kurane I. 2005. Genetic characterization of Yokose virus, a flavivirus isolated from the bat in Japan. Virology 332:38–44. http://dx.doi.org/10.1016/j.virol.2004.06.052.
22. Tilgner M, Shi PY. 2004. Structure and function of the 3′ terminal six nucleotides of the West Nile virus genome in viral replication. J. Virol. 78:8159–8171. http://dx.doi.org/10.1128/JVI.78.15.8159-8171.2004.
23. Saitou N, Nei M. 1987. The neighbor-joining method: a new method for reconstructing phylogenetic trees. Mol. Biol. Evol. 4:406–425.
24. Tamura K, Peterson D, Peterson N, Stecher G, Nei M, Kumar S. 2011. MEGA5: molecular evolutionary genetics analysis using maximum likelihood, evolutionary distance, and maximum parsimony methods. Mol. Biol. Evol. 28:2731–2739. http://dx.doi.org/10.1093/molbev/msr121.
25. Garnier J, Osguthorpe DJ, Robson B. 1978. Analysis of the accuracy and implications of simple methods for predicting the secondary structure of globular proteins. J. Mol. Biol. 120:97–120. http://dx.doi.org/10.1016/0022-2836(78)90297-8.
26. Kyte J, Doolittle RF. 1982. A simple method for displaying the hydropathic character of a protein. J. Mol. Biol. 157:105–132. http://dx.doi.org/10.1016/0022-2836(82)90515-0.
27. Zuker M. 2003. Mfold web server for nucleic acid folding and hybridization prediction. Nucleic Acids Res. 31:3406–3415. http://dx.doi.org/10.1093/nar/gkg595.
28. Okamoto K, Moriishi K, Miyamura T, Matsuura Y. 2004. Intramembrane proteolysis and endoplasmic reticulum retention of hepatitis C virus core protein. J. Virol. 78:6370–6380. http://dx.doi.org/10.1128/JVI.78.12.6370-6380.2004.
29. Okamoto T, Nishimura Y, Ichimura T, Suzuki K, Miyamura T, Suzuki T, Moriishi K, Matsuura Y. 2006. Hepatitis C virus RNA replication is regulated by FKBP8 and Hsp90. EMBO J. 25:5015–5025. http://dx.doi.org/10.1038/sj.emboj.7601367.
30. Honda M, Brown EA, Lemon SM. 1996. Stability of a stem-loop involving the initiator AUG controls the efficiency of internal initiation of translation on hepatitis C virus RNA. RNA 2:955–968.
31. Yanagi M, St Claire M, Emerson SU, Purcell RH, Bukh J. 1999. In vivo analysis of the 3′ untranslated region of the hepatitis C virus after in vitro mutagenesis of an infectious cDNA clone. Proc. Natl. Acad. Sci. U. S. A. 96:2291–2295. http://dx.doi.org/10.1073/pnas.96.5.2291.
32. Blight KJ, Rice CM. 1997. Secondary structure determination of the conserved 98-base sequence at the 3′ terminus of hepatitis C virus genome RNA. J. Virol. 71:7345–7352.
33. Friebe P, Boudet J, Simorre JP, Bartenschlager R. 2005. Kissing-loop interaction in the 3′ end of the hepatitis C virus genome essential for RNA replication. J. Virol. 79:380–392. http://dx.doi.org/10.1128/JVI.79.1.380-392.2005.
34. Lourenço S, Costa F, Debarges B, Andrieu T, Cahour A. 2008. Hepatitis C virus internal ribosome entry site-mediated translation is stimulated by cis-acting RNA elements and trans-acting viral factors. FEBS J. 275:4179–4197. http://dx.doi.org/10.1111/j.1742-4658.2008.06566.x.
35. Cristina J, del Pilar Moreno M, Moratorio G. 2007. Hepatitis C virus genetic variability in patients undergoing antiviral therapy. Virus Res. 127:185–194. http://dx.doi.org/10.1016/j.virusres.2007.02.023.
36. Song Y, Friebe P, Tzima E, Junemann C, Bartenschlager R, Niepmann M. 2006. The hepatitis C virus RNA 3′-untranslated region strongly enhances translation directed by the internal ribosome entry site. J. Virol. 80:11579–11588. http://dx.doi.org/10.1128/JVI.00675-06.
37. McLauchlan J, Lemberg MK, Hope G, Martoglio B. 2002. Intramembrane proteolysis promotes trafficking of hepatitis C virus core protein to lipid droplets. EMBO J. 21:3980–3988. http://dx.doi.org/10.1093/emboj/cdf414.
38. Ogino T, Fukuda H, Imajoh-Ohmi S, Kohara M, Nomoto A. 2004. Membrane binding properties and terminal residues of the mature hepatitis C virus capsid protein in insect cells. J. Virol. 78:11766–11777. http://dx.doi.org/10.1128/JVI.78.21.11766-11777.2004.
39. Kopp M, Murray CL, Jones CT, Rice CM. 2010. Genetic analysis of the carboxy-terminal region of the hepatitis C virus core protein. J. Virol. 84:1666–1673. http://dx.doi.org/10.1128/JVI.02043-09.
40. Weihofen A, Binns K, Lemberg MK, Ashman K, Martoglio B. 2002. Identification of signal peptide peptidase, a presenilin-type aspartic protease. Science 296:2215–2218. http://dx.doi.org/10.1126/science.1070925.
41. Barba G, Harper F, Harada T, Kohara M, Goulinet S, Matsuura Y, Eder G, Schaff Z, Chapman MJ, Miyamura T, Brechot C. 1997. Hepatitis C virus core protein shows a cytoplasmic localization and associates to cellular lipid storage droplets. Proc. Natl. Acad. Sci. U. S. A. 94:1200–1205. http://dx.doi.org/10.1073/pnas.94.4.1200.
42. Hope RG, McLauchlan J. 2000. Sequence motifs required for lipid droplet association and protein stability are unique to the hepatitis C virus core protein. J. Gen. Virol. 81:1913–1925.
43. Gao L, Aizaki H, He JW, Lai MM. 2004. Interactions between viral nonstructural proteins and host protein hVAP-33 mediate the formation of hepatitis C virus RNA replication complex on lipid raft. J. Virol. 78:3480–3488. http://dx.doi.org/10.1128/JVI.78.7.3480-3488.2004.
44. Gosert R, Egger D, Lohmann V, Bartenschlager R, Blum HE, Bienz K, Moradpour D. 2003. Identification of the hepatitis C virus RNA replication complex in Huh-7 cells harboring subgenomic replicons. J. Virol. 77:5487–5492. http://dx.doi.org/10.1128/JVI.77.9.5487-5492.2003.
45. Shi ST, Lee KJ, Aizaki H, Hwang SB, Lai MM. 2003. Hepatitis C virus RNA replication occurs on a detergent-resistant membrane that cofractionates with caveolin-2. J. Virol. 77:4160–4168. http://dx.doi.org/10.1128/JVI.77.7.4160-4168.2003.
46. Tsukiyama-Kohara K, Iizuka N, Kohara M, Nomoto A. 1992. Internal ribosome entry site within hepatitis C virus RNA. J. Virol. 66:1476–1483.
47. Babaylova E, Graifer D, Malygin A, Stahl J, Shatsky I, Karpova G. 2009. Positioning of subdomain IIId and apical loop of domain II of the hepatitis C IRES on the human 40S ribosome. Nucleic Acids Res. 37:1141–1151. http://dx.doi.org/10.1093/nar/gkn1026.
48. Kieft JS, Zhou K, Grech A, Jubin R, Doudna JA. 2002. Crystal structure of an RNA tertiary domain essential to HCV IRES-mediated translation initiation. Nat. Struct. Biol. 9:370–374. http://dx.doi.org/10.1038/nsb781.
49. Locker N, Easton LE, Lukavsky PJ. 2007. HCV and CSFV IRES domain II mediate eIF2 release during 80S ribosome assembly. EMBO J. 26:795–805. http://dx.doi.org/10.1038/sj.emboj.7601549.

50. Stewart H, Walter C, Jones D, Lyons S, Simmonds P, Harris M. 2013. The non-primate hepacivirus 5′ untranslated region possesses internal ribosomal entry site activity. J. Gen. Virol. 94:2657–2663. http://dx.doi.org/10.1099/vir.0.055764-0.
51. Diviney S, Tuplin A, Struthers M, Armstrong V, Elliott RM, Simmonds P, Evans DJ. 2008. A hepatitis C virus *cis*-acting replication element forms a long-range RNA-RNA interaction with upstream RNA sequences in NS5B. J. Virol. 82:9008–9022. http://dx.doi.org/10.1128/JVI.02326-07.
52. Penin F, Dubuisson J, Rey FA, Moradpour D, Pawlotsky JM. 2004. Structural biology of hepatitis C virus. Hepatology 39:5–19. http://dx.doi.org/10.1002/hep.20032.
53. Hirata Y, Ikeda K, Sudoh M, Tokunaga Y, Suzuki A, Weng L, Ohta M, Tobita Y, Okano K, Ozeki K, Kawasaki K, Tsukuda T, Katsume A, Aoki Y, Umehara T, Sekiguchi S, Toyoda T, Shimotohno K, Soga T, Nishijima M, Taguchi R, Kohara M. 2012. Self-enhancement of hepatitis C virus replication by promotion of specific sphingolipid biosynthesis. PLoS Pathog. 8:e1002860. http://dx.doi.org/10.1371/journal.ppat.1002860.
54. Katsume A, Tokunaga Y, Hirata Y, Munakata T, Saito M, Hayashi H, Okamoto K, Ohmori Y, Kusanagi I, Fujiwara S, Tsukuda T, Aoki Y, Klumpp K, Tsukiyama-Kohara K, El-Gohary A, Sudoh M, Kohara M. 2013. A serine palmitoyltransferase inhibitor blocks hepatitis C virus replication in human hepatocytes. Gastroenterology 145:865–873. http://dx.doi.org/10.1053/j.gastro.2013.06.012.
55. Mercer DF, Schiller DE, Elliott JF, Douglas DN, Hao C, Rinfret A, Addison WR, Fischer KP, Churchill TA, Lakey JR, Tyrrell DL, Kneteman NM. 2001. Hepatitis C virus replication in mice with chimeric human livers. Nat. Med. 7:927–933. http://dx.doi.org/10.1038/90968.

Molecules **2014**, *19*, 4006-4020; doi:10.3390/molecules19044006

OPEN ACCESS

molecules

ISSN 1420-3049

www.mdpi.com/journal/molecules

Article

PBDE: Structure-Activity Studies for the Inhibition of Hepatitis C Virus NS3 Helicase

Kazi Abdus Salam [1], Atsushi Furuta [2,3], Naohiro Noda [2,3], Satoshi Tsuneda [2], Yuji Sekiguchi [3], Atsuya Yamashita [4], Kohji Moriishi [4], Masamichi Nakakoshi [5], Hidenori Tani [6], Sona Rani Roy [7], Junichi Tanaka [7], Masayoshi Tsubuki [8,*] and Nobuyoshi Akimitsu [1,*]

1 Radioisotope Center, The University of Tokyo, 2-11-16 Yayoi, Bunkyo-ku, Tokyo 113-0032, Japan; E-Mail: salam_bio26@yahoo.com

2 Department of Life Science and Medical Bioscience, Waseda University, 2-2 Wakamatsu-cho, Shinjuku-ku, Tokyo 162-8480, Japan; E-Mails: atsushi.5961@ruri.waseda.jp (A.F.); stsuneda@waseda.jp (S.T.)

3 Biomedical Research Institute, National Institute of Advanced Industrial Science and Technology (AIST), 1-1-1 Higashi, Tsukuba, Ibaraki 305-8566, Japan; E-Mails: noda-naohiro@aist.go.jp (N.N.); y.sekiguchi@aist.go.jp (Y.S.)

4 Department of Microbiology, Graduate School of Medicine and Engineering, University of Yamanashi, 1110 Shimokato, Chuo-shi, Yamanashi 409-3898, Japan; E-Mails: atsuyay@yamanashi.ac.jp (A.Y.); kmoriishi@yamanashi.ac.jp (K.M.)

5 Faculty of Pharmaceutical Sciences, Toho University, 2-2-1 Miyama, Funabashi, Chiba 274-8510, Japan; E-Mail: nakakoshi@phar.toho-u.ac.jp

6 Research Institute for Environmental Management Technology, National Institute of Advanced Industrial Science and Technology (AIST), 16-1, Onogawa, Tsukuba, Ibaraki 305-8569, Japan; E-Mail: h.tani@aist.go.jp

7 Department of Chemistry, Biology and Marine Science, University of the Ryukyus, Nishihara, Okinawa 903-0213, Japan; E-Mails: sonarroy@gmail.com (S.R.R.); jtanaka@sci.u-ryukyu.ac.jp (J.T.)

8 Institute of Medical Chemistry, Hoshi University, Ebara 2-4-41, Shinagawa-ku, Tokyo 142-8501, Japan

* Authors to whom correspondence should be addressed; E-Mails: tsubuki@hoshi.ac.jp (M.T.); akimitsu@ric.u-tokyo.ac.jp (N.A.); Tel.: +81-3-5498-5793 (M.T.); Fax: +81-3-3787-0036 (M.T.); Tel.: +81-3-5841-2877 (N.A.); Fax: +81-3-5841-3049 (N.A.).

Received: 17 January 2014; in revised form: 5 March 2014 / Accepted: 13 March 2014 / Published: 2 April 2014

Abstract: The helicase portion of the hepatitis C virus nonstructural protein 3 (NS3) is considered one of the most validated targets for developing direct acting antiviral agents. We isolated polybrominated diphenyl ether (PBDE) **1** from a marine sponge as an NS3 helicase inhibitor. In this study, we evaluated the inhibitory effects of PBDE (**1**) on the essential activities of NS3 protein such as RNA helicase, ATPase, and RNA binding activities. The structure-activity relationship analysis of PBDE (**1**) against the HCV ATPase revealed that the biphenyl ring, bromine, and phenolic hydroxyl group on the benzene backbone might be a basic scaffold for the inhibitory potency.

Keywords: hepatitis C virus; NS3 RNA helicase; marine sponge; polybrominated diphenyl ether

1. Introduction

Hepatitis C virus (HCV) is one of the major causative agents for hepatitis C, which has caused an epidemic of liver fibrosis, cirrhosis, and hepatocellular carcinoma [1]. HCV infects more than 150 million people worldwide, and over 350,000 people die from HCV-related liver diseases each year [2]. The virus is undetectable for long periods of time, even decades, and replicates slowly without major complications. Therefore, most infected people are unaware they carry the virus. HCV is only transmitted via blood and blood products, while sexual and mother-to-child transmission is much less likely than for HIV infection [2].

The recently approved new treatment regimen for HCV infection is the combination of pegylated interferon and ribavirin with either telaprevir or boceprevir for genotype 1 infected patients. However, the emergence of viral resistance to the drugs as well as side effects, such as anemia, neutropenia, dysgeusia, rash, and anorectal discomfort, are the main concerns [3–6]. Despite intensive studies for the development of new antiviral drugs, HCV is still a major threat to human health. Therefore, there is an urgent need to develop new antiviral drugs with fewer side effects and the highest antiviral efficacy.

HCV is a single-stranded, positive-sense RNA virus in the *Flaviviridae* family [1,7]. Seven genotypes and more than 50 subtypes of HCV have been described [8]. The viral genome is 9.6 kb in length and contains one main open reading frame encoding an approximately 3,000 amino acid single polyprotein, flanked by a 5'-non-translated region (NTR) and a 3'-NTR. Once translation initiated by an internal ribosome entry site present at the 5'-NTR, host and viral proteases cleave the product into 10 individual viral mature proteins [9]. The structural proteins (envelope glycoproteins; E1 and E2) are responsible for receptor binding, thereby facilitating viral entry into the hepatocyte. The core protein (C) forms the viral nucleocapsid [10]. The nonstructural proteins p7, NS2, NS3, NS4A, NS4B, NS5A, and NS5B are involved in viral replication and packaging of the HCV genome. NS3 is a multifunctional protein that plays an important role in the viral life cycle. It has a serine protease (NS3/4A) activity at the N-terminal to cleave all downstream junctions, and helicase activity at the C-terminal to separate double-stranded RNA in a reaction fueled by ATP hydrolysis during replication of viral genomic RNA [11,12]. Although the precise role of the helicase activity in the viral life cycle

is not well understood, a fully functional helicase is essential for HCV RNA replication. The helicase portion of NS3 is thus a valid target for the development of direct acting antiviral therapy.

The development of antiviral agents for the treatment of HCV infection has been focused on small molecule inhibitors of HCV infection that can act directly on viral targets or other host target proteins critical to HCV replication. The first two approved direct acting antiviral agents, telaprevir and boceprevir, are inhibitors of the NS3/4A protease activity [13]. However, very few compounds that inhibit the NS3 helicase function have been reported, and to the best of our knowledge, no helicase inhibitors have entered clinical trials. Thus there is still a great need in HCV research to develop novel NS3 helicase inhibitors.

The aim of this project was to identify a possible NS3 helicase inhibitor from marine natural products. In this study, we successfully obtained from marine sponge and identified hydroxylated polybrominated diphenyl ether OH-PBDE-47 (**1**), as a helicase inhibitor through a high-throughput screening method based on fluorescence resonance energy transfer (FRET). We also evaluated several commercially available compounds that are structurally related to PBDE (**1**) for the study of structure-activity relationships.

PBDEs have been found to exhibit antibacterial, antifungal, and antimicroalgal activities [14–19]. They inhibit a wide range of enzymes that are relevant to anticancer drug discovery such as inosine monophosphate dehydrogenase, guanosine monophosphate synthetase, and 15-lipoxygenase [20]. PBDEs have also been shown to exhibit inhibitory activities against the assembly of microtubule protein, the maturation of starfish oocytes [21] and Tie2 kinase [22]. In this research, we found a novel activity of PBDE in the specific inhibition of HCV NS3 helicase activity.

2. Results and Discussion

To screen potential NS3 helicase inhibitors from extracts of marine organisms, we used a high-throughput fluorescence helicase assay based on FRET [23]. Out of 41 extracts isolated (Table 1), PBDE (**1**) (Figure 1) exhibited the strongest inhibition (37%) of NS3 helicase activity.

Table 1. Inhibitory effects of extracts from marine organisms on hepatitis C virus (HCV) nonstructural protein 3 (NS3) helicase activity.

No.	Sample ID	FRET (%) [a]	Possibly Contained Molecule	Species	Location
1	PM-35-1	85	misakinolide	sponge (*Theonella* sp.)	Tokashiki Island, Okinawa
2	PM-35-2	94		sponge (*Theonella* sp.)	Tokashiki Island, Okinawa
3	PM-36-1	79		gorgonian (*Euplexaura* sp.)	Tokashiki Island, Okinawa
4	PM-36-2	114		gorgonian (*Euplexaura* sp.)	Tokashiki Island, Okinawa
5	PM-37-1	93	briarane diterpenes	gorgonian (*Junceella fragilis*)	Tokashiki Island, Okinawa

Table 1. *Cont.*

No.	Sample ID	FRET (%) [a]	Possibly Contained Molecule	Species	Location
6	PM-37-2	115		gorgonian (*Junceella fragilis*)	Tokashiki Island, Okinawa
7	PM-38-1	92	hippuristanol	gorgonian (*Isis hippuris*)	Tokashiki Island, Okinawa
8	PM-38-2	112		gorgonian (*Isis hippuris*)	Tokashiki Island, Okinawa
9	PM-39-2	94		sponge (*Petrosia* sp.)	Tokashiki Island, Okinawa
10	SR-1-1	37	PBDE	sponge (*Dysidea granulosa*)	Yonaguni Island, Okinawa
11	SR-2-2	92		sponge (*Jaspis* sp.)	Yonaguni Island, Okinawa
12	SR-3-1	75	petrosynol/petrosynone	sponge (*Petrosia* sp.)	Yonaguni Island, Okinawa
13	SR-4-1	68	strongylophorines	sponge (*Strongylophora* sp.)	Yonaguni Island, Okinawa
14	SR-4-2	86		sponge (*Strongylophora* sp.)	Yonaguni Island, Okinawa
15	SR-6-1	98	sesquiterpenes	soft coral (*Clavularia* sp.)	Yonaguni Island, Okinawa
16	SR-8-1	98		soft coral (*Parerythropodium* sp.)	Yonaguni Island, Okinawa
17	SR-8-2	84		Yonaguni Island, Okinawa	Yonaguni Island, Okinawa
18	SR-10-1	112	polyketide peroxides	sponge (*Plakortis* sp.)	Yonaguni Island, Okinawa
19	SR-11-1	65		sponge (unidentified)	Yonaguni Island, Okinawa
20	SR-12-2	135		sponge (unidentified)	Yonaguni Island, Okinawa
21	SR-13-2	109		sponge (*Pseudoceratina purpurea*)	Yonaguni Island, Okinawa
22	SR-14-1	64	swinholide	sponge (*Theonella swinhoei*)	Yonaguni Island, Okinawa
23	SR-15-1	61		sponge (unidentified)	Yonaguni Island, Okinawa
24	SR-16-1	92		sponge (unidentified)	Yonaguni Island, Okinawa
25	SR-17-2	87		sponge (unidentified)	Yonaguni Island, Okinawa
26	SR-19-2	131		sponge (*Hyrtios* sp.)	Yonaguni Island, Okinawa

Table 1. *Cont.*

No.	Sample ID	FRET (%) [a]	Possibly Contained Molecule	Species	Location
27	SR-21-1	155	xestospongin	sponge (*Xestospongia* sp.)	Yonaguni Island, Okinawa
28	SR-21-2	156		sponge (*Xestospongia* sp.)	Yonaguni Island, Okinawa
29	SR-23-1	73	avarol	sponge (*Dysidea arenaria*)	Yonaguni Island, Okinawa
30	SR-23-2	82		sponge (*Dysidea arenaria*)	Yonaguni Island, Okinawa
31	SR-24-1	123	isocyanosesquiterpenes	sponge (*Theonella* sp.)	Yonaguni Island, Okinawa
32	SR-26-2	102		sponge (unidentified)	Yonaguni Island, Okinawa
33	SR-27-1	188		sponge (*Leucetta* sp.)	Yonaguni Island, Okinawa
34	SR-27-2	171		sponge (*Leucetta* sp.)	Yonaguni Island, Okinawa
35	SR-28-1	107		sponge (unidentified)	Yonaguni Island, Okinawa
36	SR-29-2	145		sponge (*Aaptos* sp.)	Yonaguni Island, Okinawa
37	SR-30-2	215	agelasine	sponge (*Agelas* sp.)	Yonaguni Island, Okinawa
38	SR-31-1	100	hippuristanol	gorgonian (*Isis hippuris*)	Yonaguni Island, Okinawa
39	SR-33-2	88		sponge (unidentified)	Yonaguni Island, Okinawa
40	SR-34-1	125		zoanthus (*Palythoa* sp.)	Yonaguni Island, Okinawa
41	SR-34-2	124	palytoxin	zoanthus (*Palythoa* sp.)	Yonaguni Island, Okinawa

[a] NS3 activity in the presence of marine organisms extract is expressed as a percentage of the control in the absence of extract (100%).

Figure 1. Chemical structure of PBDE (**1**).

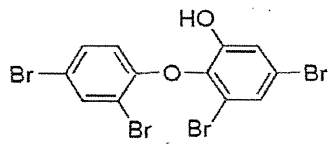

1

NS3 helicase hydrolyzes ATP as an energy source to drive the unwinding of dsRNA or dsDNA. Therefore, we measured the inhibitory effects of PBDE (**1**) on the ATPase activity of the helicase portion of NS3. A radioisotope labeling ATPase assay showed that PBDE (**1**) inhibited the hydrolytic release of inorganic phosphate from ATP with an IC_{50} of 80 μM (Figure 2A,B).

Figure 2. PBDE (**1**) inhibits NS3 ATPase activity. (**A**) Radioisotope labeling ATPase assay with NS3 (300 nM) and various concentrations of PBDE. Lane 1 shows the negative control reaction. Lanes 2–3 show the reaction mixture containing only NS3 and DMSO. Lanes 4–17 show hydrolytic reactions with NS3 (300 nM) in the presence of PBDE as indicated. (**B**) Graphical representation of the inhibition results. The relative ATPase activity for control reactions was considered as 100%. The average values are presented with error bars from duplicate assays.

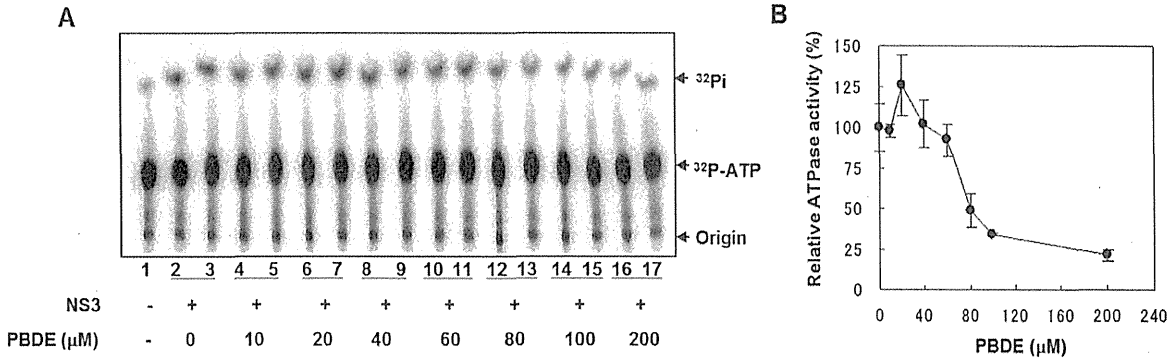

To examine the specificity of PBDE (**1**) for the inhibition of ATPase activity, we evaluated the ATP hydrolytic effect on bacterial alkaline phosphatase. PBDE (**1**) exhibited no inhibition (Figure 3), indicating that the inhibitory activity of PBDE (**1**) is specific to NS3.

Figure 3. Effect of PBDE (**1**) on the ATPase activity of bacterial alkaline phosphatase. The assay was conducted in the absence (DMSO) or presence of PBDE (**1**) (at the highest concentration tested, 200 μM). The data are expressed as the mean of three replicates with error bars representing standard deviation.

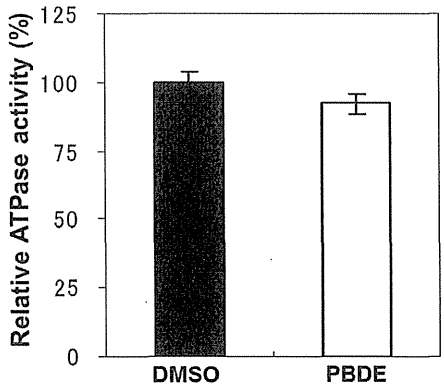

The binding of NS3 to ssRNA is required to initiate the unwinding activity of dsRNA during viral replication. We employed a gel mobility shift assay to characterize the inhibition of NS3 binding to RNA. PBDE (**1**) inhibited RNA binding of NS3 in a dose-dependent manner with an IC_{50} of 68 μM (Figure 4A,B). Previous reports indicate that poly(U) RNA enhances the ATPase activity of NS3 [24]. Because PBDE (**1**) inhibits the RNA binding ability of NS3, we speculated that inhibition of NS3 ATPase activity by PBDE (**1**) could be mediated through the inhibition of poly(U) RNA binding.

Therefore, we next performed ATPase assays including poly(U) RNA to determine the effects of poly(U) with PBDE (**1**) near to its IC_{50} concentration. We found that PBDE (**1**) was significantly active in both the presence and absence of poly(U) (Figure 5A,B), suggesting that poly(U) has no effect on the ATPase inhibition mediated by PBDE (**1**). These results are consistent with our previous data (Figure 2B).

Figure 4. PBDE (**1**) inhibits NS3 RNA binding. (**A**) Gel mobility shift assay to characterize the inhibition of NS3 binding to [γ-^{32}P] labeled ssRNA. RNA only control (lane 1), 300 nM BSA instead of NS3 control (lane 2), NS3 protein (300 nM) and DMSO control (lane 3), and NS3 protein with increasing concentrations of PBDE (**1**) (lanes 4–8). (**B**) Graphical representation of the RNA binding inhibition shown in panel A.

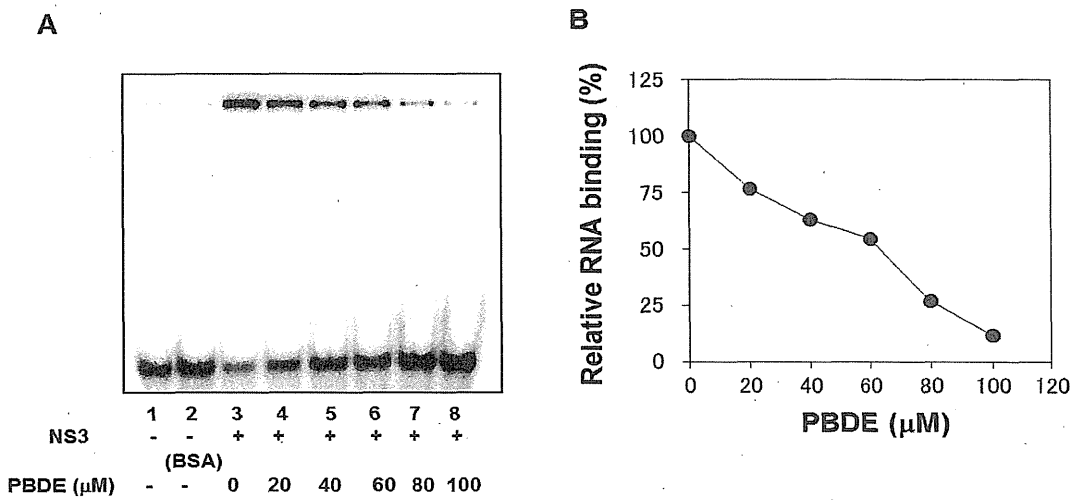

Figure 5. Effect of poly(U) RNA on NS3 ATPase activity. (**A**) ATPase assay with hydrolytic reaction buffer containing NS3 (600 nM), 1 mM [γ-^{32}P] ATP, poly(U) RNA and PBDE (0.1 mM) as indicated. (**B**) Graphical representation of data presented in (A). The solid and white bars represent NS3 and poly(U) ATPase reactions performed with DMSO and PBDE (**1**), respectively. The assay was performed in triplicate and data are presented as mean ± standard deviation. * $p > 0.05$ and ** $p > 0.01$ from Student *t*-test.

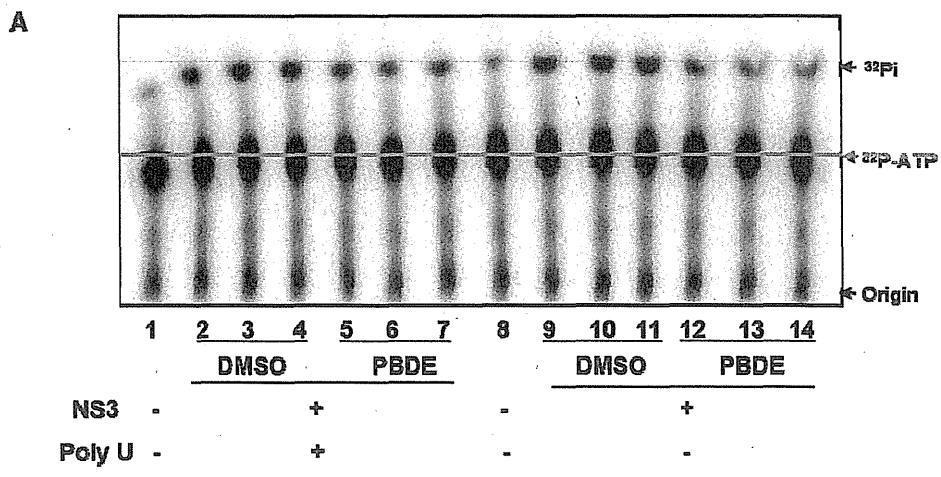

Figure 5. *Cont.*

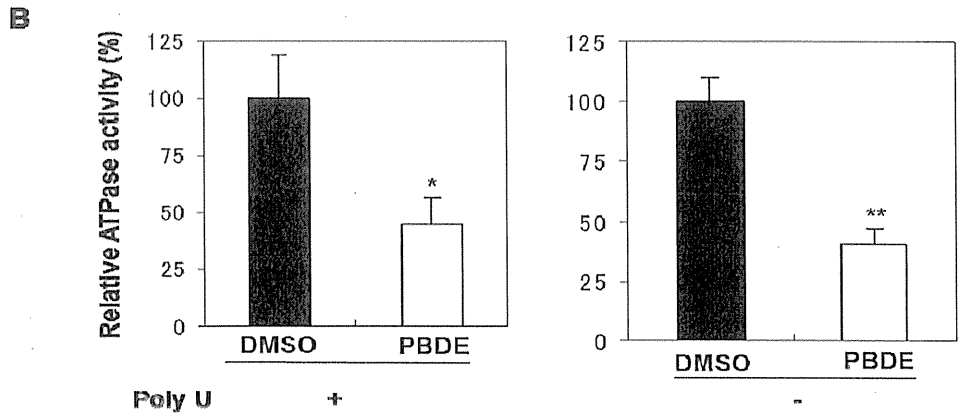

To clarify the structure-activity relationships of PBDE for inhibition of the ATPase activity of the NS3 protein, commercially available and natural phenol derivatives were examined (Table 2). We first investigated whether the hydroxyl group of PBDE (**1**) is required for ATPase activity. Substituting a methoxy group [25] (*i.e.*, PBDE methyl ether **2**) and a hydrogen (*i.e.*, deoxy PBDE **17**), for a phenolic hydroxyl group in PBDE led to a complete loss of the inhibitory activity. These findings indicated that the phenolic hydroxyl group has important effects on the inhibitory activity. Triclosan (**4**), which is structurally very close to PBDE, showed moderate levels of inhibition, indicating that bromine substituents on benzene rings can be replaced by chlorine substituents.

Table 2. Inhibition of the ATPase activity of the NS3 protein by PBDE (**1**) and its structurally related compounds.

Compound No.	Chemical Structure (PBDE/related compounds)	NS3 ATPase Inhibition IC_{50} (μM)
1	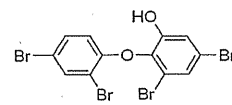	80
2	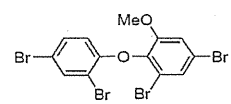	>200
3	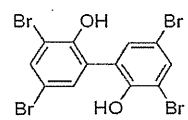	94
4	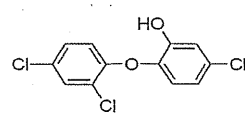	150
5	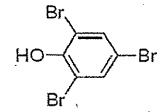	>200

Table 2. *Cont.*

Compound No.	Chemical Structure (PBDE/related compounds)	NS3 ATPase Inhibition IC_{50} (μM)
6	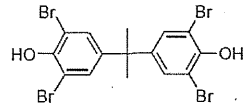	120
7	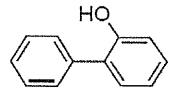	>200
8	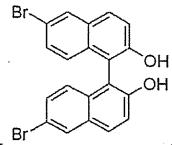	54
9	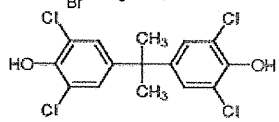	94
10	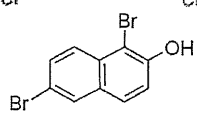	>200
11	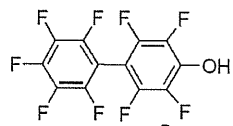	>200
12	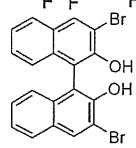	>200
13	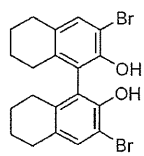	>200
14	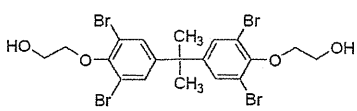	>200
15	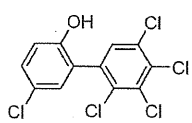	54
16	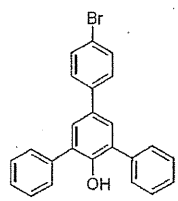	>200
17	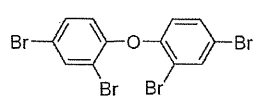	>200

Next, we took into consideration the size of the structural motif [biphenyl (compounds **3**,**7**,**11**,**15**) compared to phenyl (compound **5**) and fused ring (compound **10**)]. Interestingly, the inhibitory activity of bromophene **3**, a biphenyl derivative possessing bromine and phenolic hydroxyl groups, remained at the same level as that of PBDE (**1**). While *o*-hydroxybiphenyl **7** showed loss of the inhibitory activity, hydroxyl-pentachlorobiphenyl **15** displayed the most potent inhibitory activity of all the analogs in this study. Notably, an additional halogen substituent on the benzene ring led to a nearly two-fold increase in activity over bromophene **3**.

Furthermore, hydroxynonafluorobiphenyl **11** was also inactive. These findings suggested that both halogen, such as bromine and chlorine, and phenolic hydroxyl groups on benzene rings would be crucial for the inhibition of the ATPase activity of the NS3 protein. Unfortunately, tribromophenol **5** and dibromonaphthalenol **10** did not exhibit the inhibitory activity, indicating that the molecular frame could affect the activity level. Tetrahalobisphenols A, (compounds **6** and **9**), showed the same level of inhibition as that of bromophene **3**. Replacement of methoxy groups in tetrabromobisphenol A (**6**) with 2-hydroxyethoxy groups, *i.e.*, the bisphenol A hydroxyethyl ether **14**, brought about loss of activity. Dibromobinaphthol **8**, a dimer of bromonaphthalenol **10**, displayed the most potent activity, whereas isomeric bromobinaphthol **12** and tetrahydrobromobinaphthol **13** showed no activity. These findings indicated that the distance between halogen and phenolic hydroxyl groups has important effects on the inhibitory activity. 4-Bromophenyl-2,6-diphenylphenol **16** did not show inhibitory activity likely because of the steric hindrance around the phenolic hydroxyl group.

The log P is a measure of the lipophilicity of an organic compound, and can be defined as the ratio of the concentration of the unionized compound at equilibrium between organic and aqueous phases. Studies have shown that many biological phenomena can be correlated with this parameter, such that structure-activity relationships may be deduced. The relationship between the IC_{50} and log P of PBDE and its structurally related compounds **1**–**17** is shown in Figure 6. Biphenyl ethers **1** and **4**, biphenyls **3** and **15**, tetrahalobisphenols A **6** and **9**, and binaphthol **8** with a log P of over approximately 5 were located at the upper left, indicating the inhibitory activity. The inhibitory potency of halogenated phenols on the ATPase might increase with growing lipophilicity. Therefore, we have identified PBDE (**1**) and related compounds, hydroxypentachlorobiphenyl and dibromobinaphthol, as potent inhibitors of the HCV ATPase.

Figure 6. The relationships between Log P and IC_{50} values of the compounds.

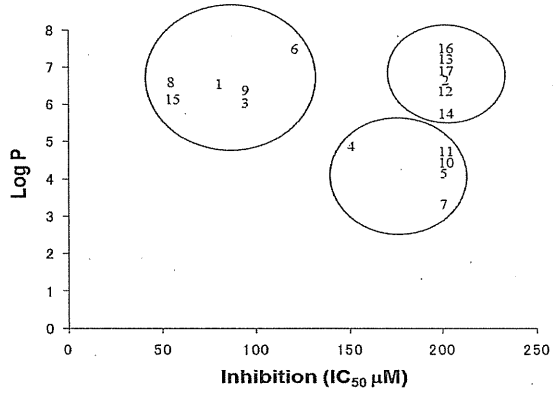

Finally, we examined the effects of PBDE (**1**) on HCV replication. As shown in Figure 7, PBDE (**1**) suppressed HCV replication in a dose-dependent manner (EC_{50} = 3.3 μM) without cytotoxic effect (CC_{50} > 5 μM).

Figure 7. Effect of PBDE (**1**) on viral replication. The subgenomic replicon RNA of genotype 1b N strain was incubated in medium containing various concentrations of PBDE (**1**) or DMSO. Luciferase and cytotoxicity assays were carried out as described in Experimental section. Error bars indicate standard deviation. The data represent three independent experiments.

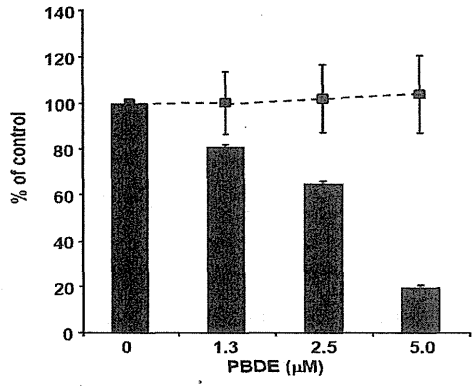

3. Experimental

3.1. Chemicals and Reagents

The γ-^{32}P-ATP isotope was purchased from Muromachi Yakuhin (Tokyo, Japan). Oligonucleotides were synthesized by Gene Design Inc. (Osaka, Japan). Bacterial alkaline phosphatase (BAPC75) was purchased from Takara Bio (Otsu, Japan). 6-hydroxy-2,2',4,4'-tetrabromodiphenyl ether (PBDE, **1**) was isolated from a marine sponge, and compound **2** was obtained by methylation of compound **1** with trimethylsilyldiazomethane. Bromophene **3**, triclosan (**4**), 2,4,6-tribromophenol (**5**), 3,3',5,5'-tetrabromobisphenol A (**6**), *O*-hydroxybiphenyl (**7**), 1,6-dibromo-2-naphthol (**10**), and 4,4'-isopropylidenebis[2-(2,6-dibromophenoxy)ethanol] (**14**) were purchased from Wako Pure Chemical (Osaka, Japan). Poly(U) RNA, 2,3,5,6-tetrafluoro-4-(pentafluorophenyl)phenol (**11**), (*R*)-(+)-3-3'-dibromo-1,1'-bi-2-naphthol (**12**), (*R*)-(+)-3,3'-dibromo-5,5',6,6',7,7',8,8'-octahydro-1,1'-bi-2,2'-naphthalenediol (**13**), and 4-(4-bromophenyl)-2,6-diphenylphenol (**16**) were obtained from Sigma-Aldrich (St. Louis, MO, USA). (*R*)-(−)-6,6'-dibromo-1,1'-bi-2-naphthol (**8**) and tetrachlorobisphenol A (**9**) were purchased from TCI (Tokyo, Japan). 2-Hydroxy-2',3',4',5,5'-pentachlorobiphenyl (**15**) and 2,2',4,4'-tetrabromodiphenyl ether (**17**) were obtained from AccuStandard (New Haven, CT, USA).

3.2. Extraction of PBDE

The specimens used in this study were collected from marine organisms near Okinawa Islands, Japan (Table 1). Extractions were performed three times with either ethanol or acetone, and the ethyl-soluble portions (PM/SR-*-1) were obtained after concentration and partition. The aqueous layer